A 2D Layered Fluorescent Crystalline Porous Organic Salt

Danling Sun,[ab] Guolong Xing,*[ab] Jie Lyu,[ab] Yuxia Han,[ab] Pu Sun,[ab] Yu Zhao,[ab] Kanwal Iqbal,[ac] Huating Kong,[d] Yuanbin Zhang,[b] Daoling Peng,*[e] Bo Song,[f] Weidong Zhu,[ab] Teng Ben*[ab]

[a]Zhejiang Engineering Laboratory for Green Syntheses and Applications of Fluorine-Containing Specialty Chemicals, Institute of Advanced Fluorine-Containing Materials, Zhejiang Normal University, Jinhua, 321004, P. R. China
[b]Key Laboratory of the Ministry of Education for Advanced Catalysis Materials, Institute of Physical Chemistry, Zhejiang Normal University, Jinhua, 321004, P. R. China
[c]Department of Chemistry, Sardar Bahadur Khan Women's University, Quetta, 87300, Pakistan
[d]Shanghai Synchrotron Radiation Facility, Shanghai Advanced Research Institute, Chinese Academy of Sciences, Shanghai, 201204, P. R. China
[e]Key Laboratory of Theoretical Chemistry of Environment, Ministry of Education, School of Environment, South China Normal University, Guangzhou, 510006, P. R. China
[f]School of Optical-Electrical Computer Engineering, University of Shanghai for Science and Technology, Shanghai, 200093, P. R. China
*e-mail: xinggl@zjnu.edu.cn; pengdaoling@m.scnu.edu.cn; tengben@zjnu.edu.cn

Contents

Section 1. Materials and Methods

$LiCl·H_2O$ (99%), $CrCl_3·6H_2O$ (99.5%), $CeCl_3$ (99%), $NdCl_3$ (99%), $DyCl_3$ (99%), $LuCl_3·6H_2O$ (99%) were purchased from Bide Pharmatech Co., Ltd. KCl (99.5%), $CoCl_2·6H_2O$ (99%), $CdCl_2·2.5H_2O$ (99%), $MgCl_2$ (99%), $NiCl_2$ (Ni＞42%), $SmCl_3·6H_2O$ (99%), $TmCl_3·6H_2O$ (99%), $PrCl_3·6H_2O$ (99%), $HoCl_3·6H_2O$ (99%) were purchased from Shanghai Titan Scientific Co., Ltd. NaCl (99.5%) was purchased from Shanghai Lianshi Chemical Reagent Co., Ltd. $CaCl_2$ (AR) was purchased from Sinopharm Chemical Reagent Co., Ltd. All other reagents and solvents are commercially available and were used as received.

Solution ^1H nuclear magnetic resonance (NMR) spectra were performed on a Bruker UltraShield 400 NMR spectrometer. Chemical shifts are reported in parts per million (ppm) referenced to residual solvent protons. The Fourier transform infrared (FT-IR) spectra were recorded in ATR mode at room-temperature on a Thermo Scientific Nicolet iS50 in the range 400-4000 cm^{-1}. The thermogravimetric analysis (TGA) was carried out with a NETZSCH-400 STA 449C over the temperature range from R.T to 900 ^oC at a heating rate of 10 ^oC min^{-1} in dried air atmosphere with an air flow rate of 30 mL min^{-1} using an empty Al_2O_3 crucible as the reference. Prior to TGA test, the samples were dried under vacuum for 10 hours at 120 ^oC. Field emission scanning electron microscopies (FE-SEM) were carried out using a ZEISS Gemini SEM 300 operating at an accelerating voltage of 10.0 kV. The powder X-ray diffraction (PXRD) pattern of CPOS-9 was recorded on Bruker D8 Advance using Cu-Kα radiation (40 kV, 40 mA) over a range of 2θ = 2.0-40.0^o. The Ultraviolet-visible spectroscopy (UV-vis) were recorded at room-temperature on a SHIMADZU UV-2700 in the range 190-800 nm. CO_2 sorption experiments at 273 K up to 1 bar were collected using an iPore400 surface area and pore size analyzer. Before sorption analysis, the sample was degassed at 150 ^oC for 8 hours under vacuum. To measure the free space, He of 99.99% purity was used and it was presumed that He was not adsorbed at any temperature in which the experiments were accomplished. CO_2 isotherm measurements at 273 K were carried out in an ice-water bath. The Micropore Surface Area and Pore size were calculated by iPoreDFT software. The fluorescence spectra were obtained by EDINBURGH FLS920 Combined Steady-state and lifetime fluorescence Spectrometer. Dynamic light scattering (DLS) analysis was carried out with a Zetasizer Nano ZS90 at room temperature.

Crystallographic data were collected from a single crystal at 298.0 K on a XtaLAB Pro II AFC12 (RINC): Kappa single four-circle diffractometer with a micro-focus sealed X-ray tube using a mirror as monochromator. The diffractometer was equipped with a low temperature device and used CuK_α radiation (λ = 1.54184 Å). All data were integrated with Crysalispro and a multi-scan absorption correction using SCALE3 ABSPACK was applied.[S1] The structure was solved by direct methods using SHELXT and refined by full-matrix least-squares methods against F^2 by ShelXL using Olex2.[S2-S4] All non-hydrogen atoms were refined with anisotropic displacement parameters. All C-bound hydrogen atoms were refined isotropic on calculated positions using a riding model with their U_{iso} values constrained to 1.5 times the U_{eq} of their pivot atoms for terminal sp^3 carbon atoms and 1.2 times for all other carbon atoms. Disordered moieties

were refined using bond lengths restraints and displacement parameter restraints. Crystallographic data for the structures reported here have been deposited with the Cambridge Crystallographic Data Centre.[S5] CCDC 2361305 contain the supplementary crystallographic data for this paper. These data can be obtained free of charge from The Cambridge Crystallographic Data Centre via www.ccdc.cam.ac.uk/structures.

Fluorescence Measurement. In a typical experiment, CPOS-9 is suspended in ethanol and sonicated for 6 hours to achieve a uniform suspension at a concentration of 0.05 mg/mL. After aging for 10 minutes at room temperature to form a stable suspension, the mixture is sonicated again to ensure uniform dispersion. A series of MCl_x solutions (10 mM, M = Li^+, Na^+, K^+, Mg^{2+}, Ca^{2+}, Co^{2+}, Ni^{2+}, Zn^{2+}, Cd^{2+}, Nd^{3+}, Dy^{3+}, Ce^{3+}, Lu^{3+}, Sm^{3+}, Tm^{3+}, Pr^{3+}, Ho^{3+}, Cr^{3+}, where the counterion is Cl^-) are prepared. Subsequently, 300 μL of the CPOS-9 suspension and 30 μL of the MCl_x solution are combined in a 350 μL quartz cell, and their fluorescence spectra are collected at an excitation wavelength of 340 nm.

Limit of detection. A series of samples are prepared by mixing the CPOS-9 suspension with a Ce^{3+} solution, with concentrations ranging from 0 to 100 μM. After thorough mixing, the mixtures are allowed to stand for a specified period to ensure equilibrium before fluorescence spectra are measured. A calibration curve is established based on the fluorescence intensity at 340 nm, which correlates with the Ce^{3+} content. To determine the detection limit, a blank sample is prepared by mixing 300 μL of the CPOS-9 suspension with 30 μL of deionized water, and its fluorescence intensity is measured similarly.

Interference experiment. In a typical experiment, 30 μL of a solution containing other interference ion (20 mM), with a concentration double that of the Ce^{3+} solution (10 mM), is added to 300 μL of the CPOS-9 suspension. Subsequently, the Ce^{3+} solution is added, and the resulting fluorescence spectra are collected.

Method of DFT calculations. An representative fragment (F) of the CPOS-9 and ion complexes (F-Ce^{3+}) were calculated separately in DFT formalism with 6-311G(d,p) basis set and the popular B3LYP functional. Due to the symmetry of CPOS-9 crystal, the symmetry inequivalent fragment including one $TAmPE^{4+}$ cation and two $BPDS^{2-}$ anions was taken as the representative computing model. To evade the computational cost, effective core potential (ECP) of SDD model was employed for the cerium atom. The electronic structure calculations including DFT and TDDFT methods were performed by using the Gaussian16 software package. In case of F-Ce^{3+}, unrestricted DFT method was employed, and the lowest energy configuration was analyzed for the present study. The calculated transitions are shown in the following Table S1 and S2, where the molecular orbitals (MOs) involved in major components of the transitions for F and F-Ce^{3+} are shown. It should be noted that in each case, the transition involves $\pi \rightarrow \pi^*$ MOs. The experimentally found absorption band at 436 nm and 460 nm are corresponding to the electronic transition between inner orbitals with significant oscillator strength. The orbital transitions corresponding to oscillator strength higher than 0.004 are taken into account and are summarized in Table S3.

Section 2. Synthetic Procedures

Tetrakis(4-amidinophenyl)ethylene hydrochloride (TAmPE·4HCl)

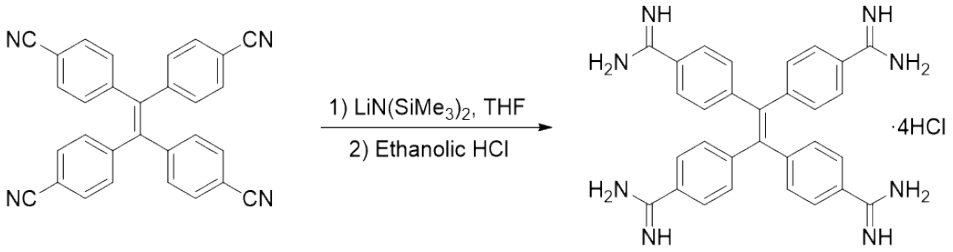

Scheme S1. Synthesis of TAmPE·4HCl.

Tetrakis(4-amidinophenyl)ethylene hydrochloride (TAmPE·4HCl) was synthesized according to the previous literature.[S6] Tetra(4-cyanophenyl)ethylene (2.4 g, 5.6 mmol) was dissolved in dry THF (180 mL) at -40 °C under a nitrogen atmosphere, and LiHMDS solution (1.0 M in THF, 111 mL, 111 mmol) was added dropwise. The mixture was allowed to warm to room temperature and stirred overnight. The reaction mixture was cooled to 0 °C and ethanolic HCl (prepared by cautiously adding 30.0 mL of acetyl chloride to 100 mL ethanol) was added slowly, which resulted in the formation of a pale precipitate. The precipitate was then evaporated to dryness in vacuo, and the solid was dissolved in H_2O (100 mL) and NaOH (0.9 g, 22.5 mmol). The solution was filtered, concentrated hydrochloric acid (8 mL) and ethanol (50 mL) was added to the solid, the solution was filtered to give TAmPE·4HCl as a pale solid (2.9 g, 81.0%).

Synthetic procedure for CPOS-9. TAmPE·4HCl (12.9 mg, 0.02 mmol) was dissolved in a mixture of 1,4-dioxane (2 mL) and distilled water (6 mL) in a 20 mL vial. BPDS (12.6 mg, 0.04 mmol) was dissolved in a mixture of 1,4-dioxane (2 mL) and distilled water (2 mL) in another 20 mL vial. Subsequently, the TAmPE·4HCl solution was added dropwise to BPDS solution. The sealed vial was left undisturbed at room temperature for 12 hours and fine rod-like colorless crystals obtained. The crystal was filtrated, and washed with a solution of 1,4-dioxane and water (1:3 ratio by volume). The target product was isolated and dried under vacuum for 10 hours at 120 °C to afford CPOS-9 as a light-yellow powder (9.4 mg, 49.8%).

Section 3. NMR Spectra

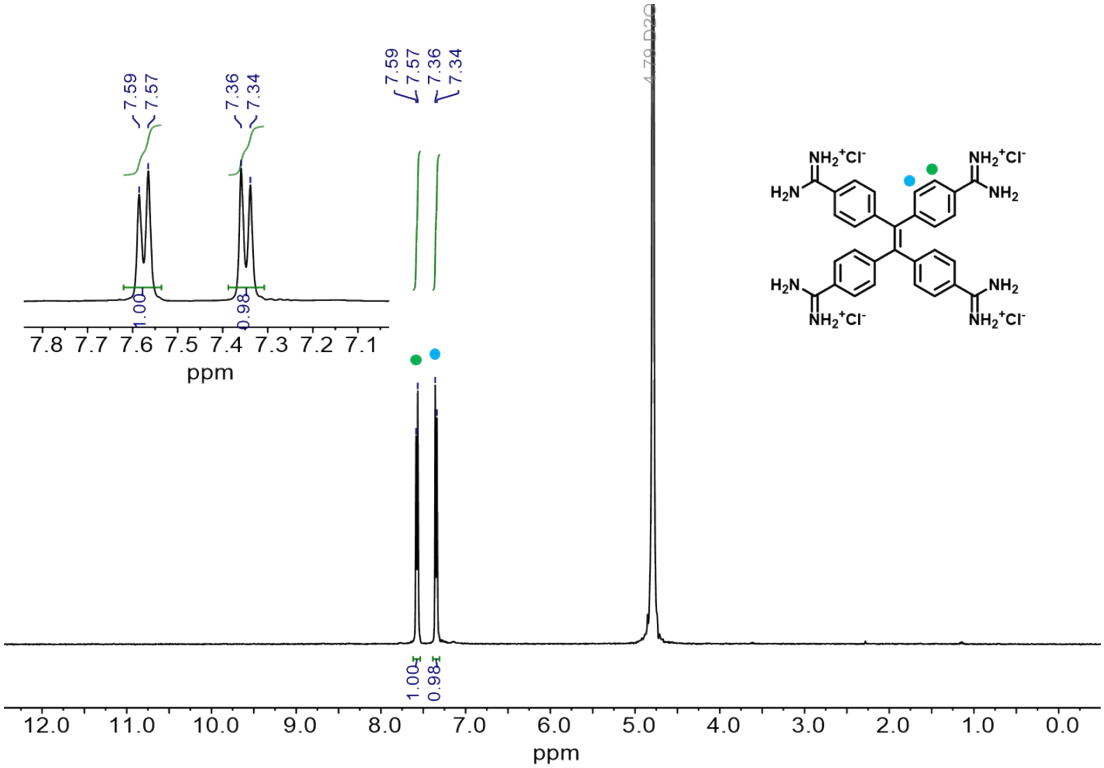

Fig. S1. ^{1}H NMR spectrum of TAmPE·4HCl in D_2O at room temperature.

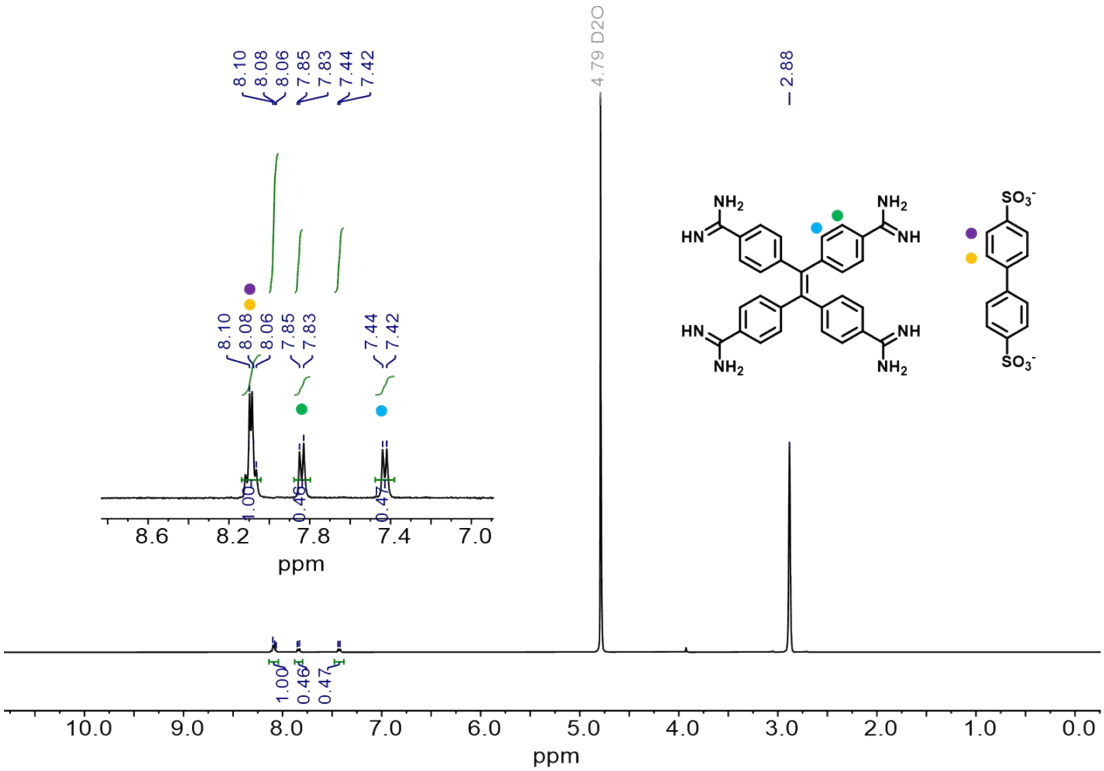

Fig. S2. ^{1}H NMR spectrum of CPOS-9 destroyed by NaOH in a mixture of D_2O and DMSO-d_6 at room temperature.

Section 4. Structure of $TAmPE^{4+}$ in CPOS-9

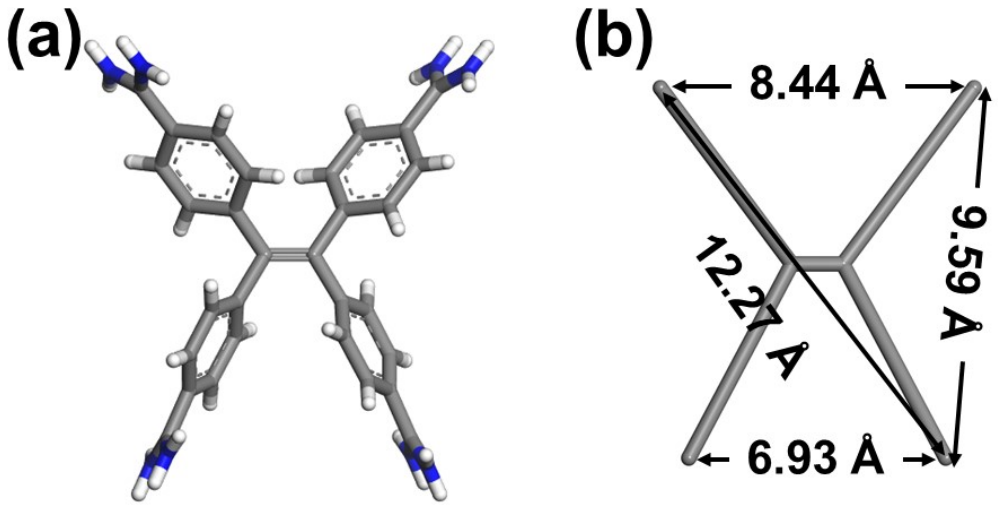

Fig. S3. Structural representation of $TAmPE^{4+}$ within CPOS-9 and the distance between the positive charges.

Section 5. PXRD Patterns

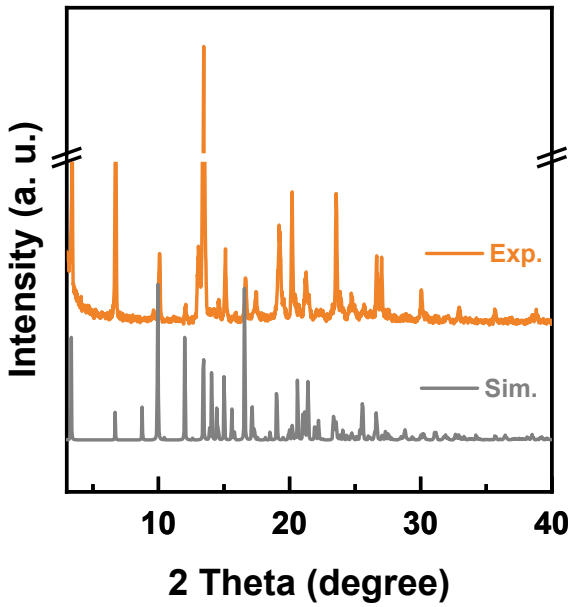

Fig. S4. Experimental (orange) and simulated (grey) PXRD patterns of CPOS-9.

Section 6. SEM Image

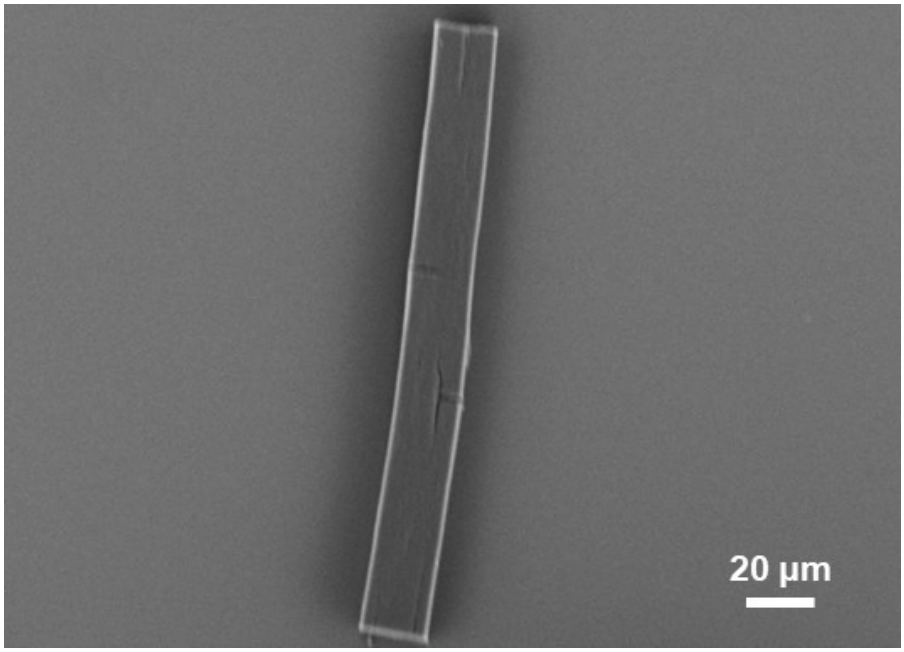

Fig. S5. SEM image of CPOS-9.

Section 7. N_2 Adsorption Isotherm

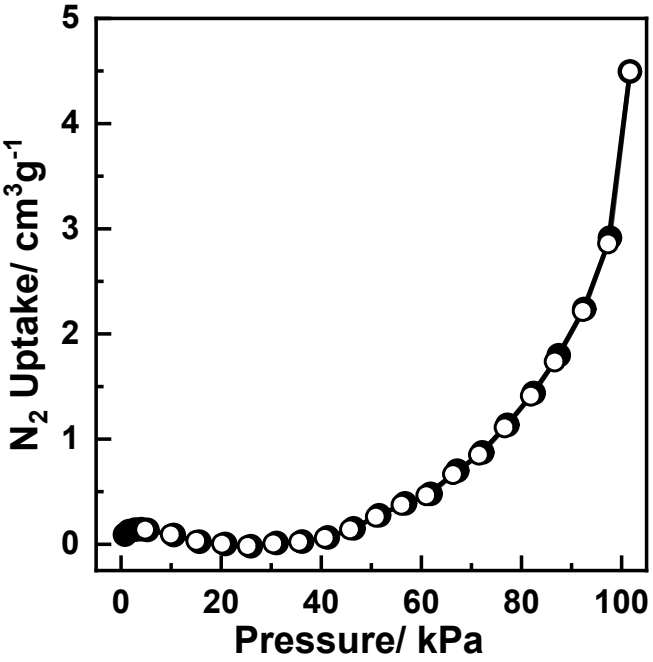

Fig. S6. N_2 sorption isotherm of CPOS-9 at 77K.

Section 8. Homogeneous Suspension

Fig. S7. Tyndall Effect in the homogeneous suspension of CPOS-9.

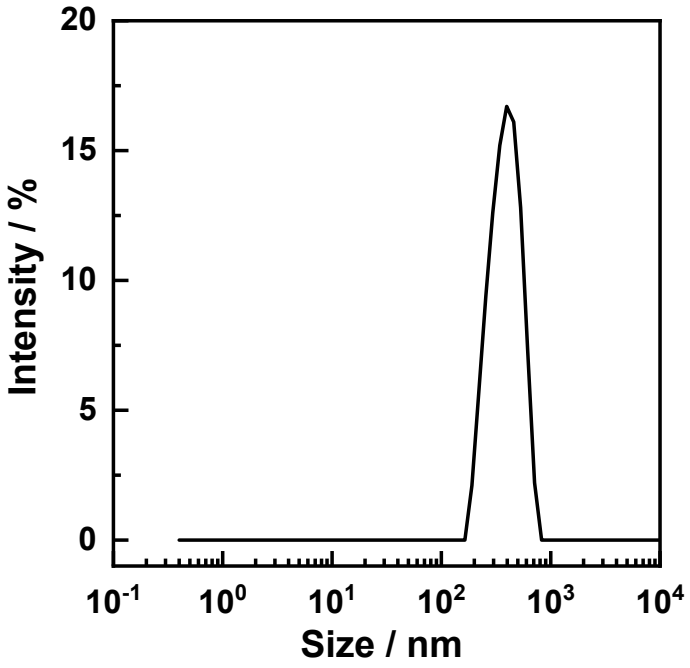

Fig. S8. Particle size distributions of CPOS-9 in ethanol.

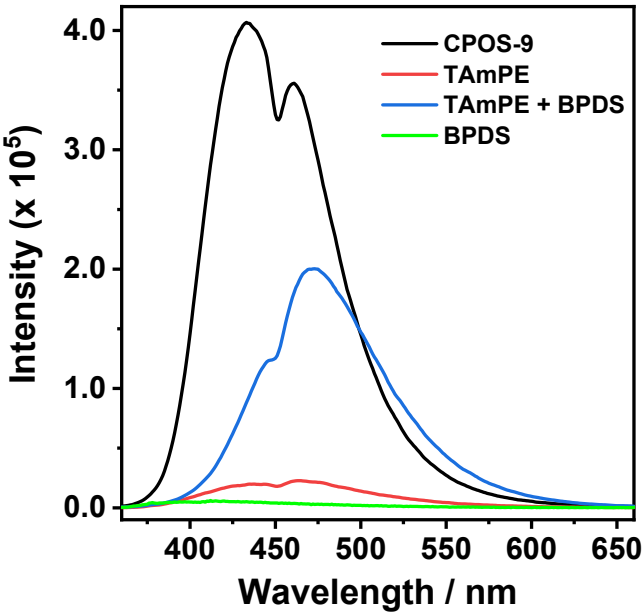

Fig. S9. The fluorescent property of CPOS-9, BPDS, TAmPE, and the mixture of BPDS and TAmPE in ethanol solution under the same condition.

Section 9. Stability of CPOS-9 for detecting Ce^{3+}

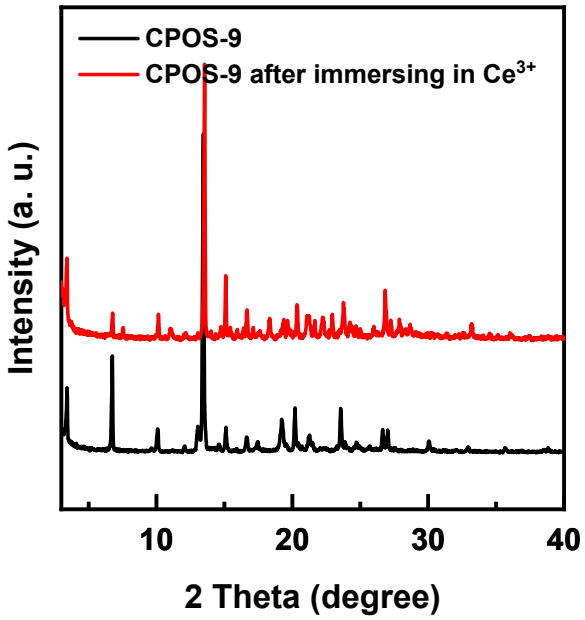

Fig. S10. PXRD patterns of CPOS-9 before and after immersing in Ce^{3+} solution.

Section 10. Theoretical Calculations

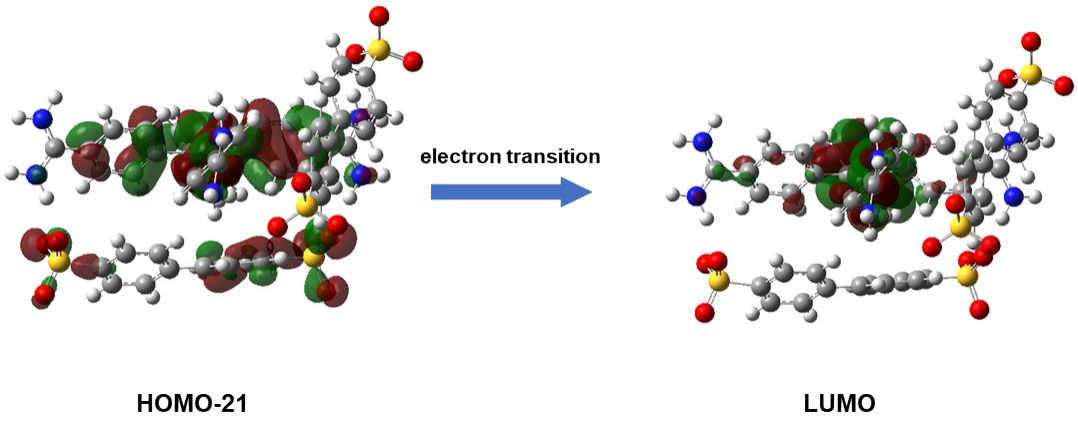

Fig. S11. Electron transition between HOMO-21 and LUMO orbits of CPOS-9 in another direction.

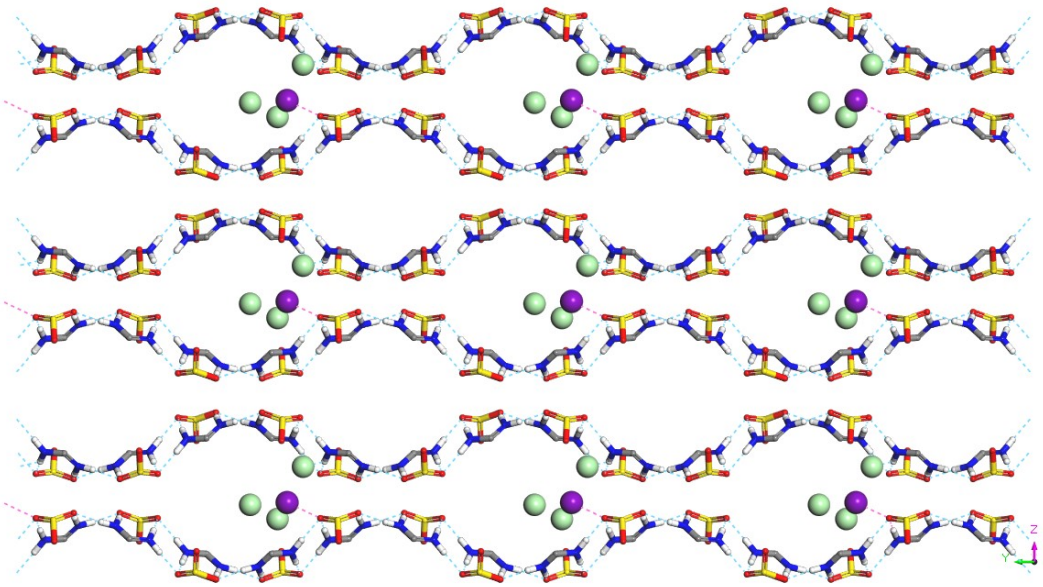

Fig. S12. Adsorption site of Ce^{3+} in the cavity of CPOS-9. (C: gray; N: blue; O: red; S: yellow; H: white; Ce: purple; Cl: Green)

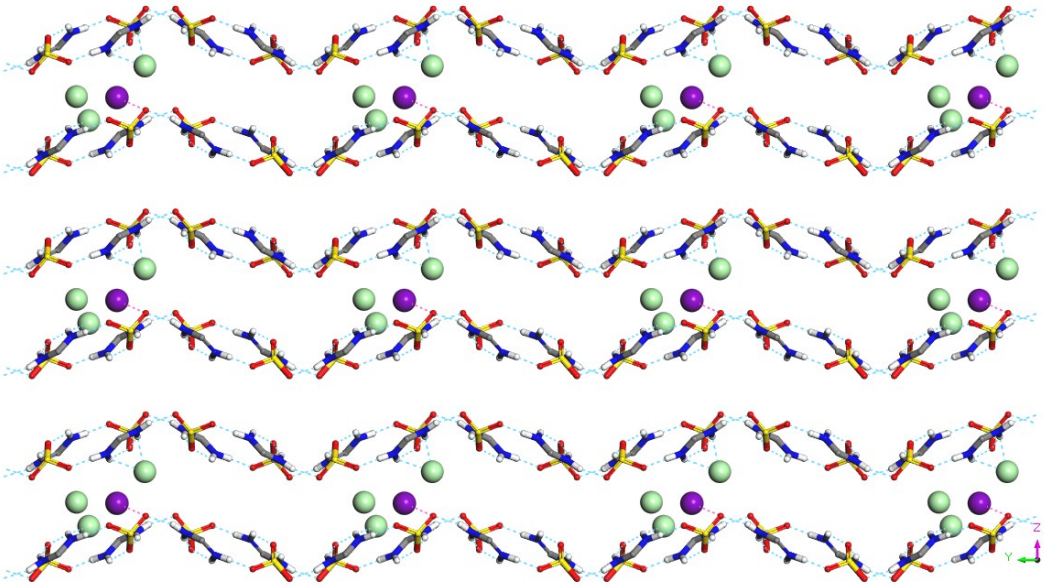

Fig. S13. Adsorption site of Ce^{3+} in the channel of CPOS-9. (C: gray; N: blue; O: red; S: yellow; H: white; Ce: purple; Cl: Green)

Table S1. The wavelength (nm), most dominant orbital transition and oscillator strength (a. u.) calculated for molecule F.

Wavelength (nm)	Most dominant orbital transition	Oscillator strength
390	HOMO-21 to LUMO+1	0.0062
406	HOMO-13 to LUMO+1	0.0315
411	HOMO-13 to LUMO+1 HOMO-11 to LUMO+1	0.0061
431	HOMO-11 to LUMO HOMO-21 to LUMO	0.1931
458	HOMO-11 to LUMO HOMO-21 to LUMO	0.2053
513	HOMO-6 to LUMO+1 HOMO-1 to LUMO	0.0043
595	HOMO-1 to LUMO+1 HOMO-1 to LUMO	0.0102

Table S2. The wavelength (nm), most dominant orbital transition and oscillator strength (a. u.) calculated for molecule F-Ce^{3+}.

Wavelength (nm)	Most dominant orbital transition	Oscillator strength
391	HOMO-21 to LUMO+1	0.0072
407	HOMO-13 to LUMO+1	0.0472
413	HOMO-13 to LUMO+1 HOMO-11 to LUMO+1	0.0072
430	HOMO-11 to LUMO HOMO-21 to LUMO	0.1081
458	HOMO-11 to LUMO HOMO-21 to LUMO	0.1364
512	HOMO-6 to LUMO+1 HOMO-1 to LUMO	0.0067
594	HOMO-1 to LUMO+1 HOMO-1 to LUMO	0.0249

Table S3. Ground state density plot and energies (eV) of the frontier molecular orbitals of molecule F.

Wavelength (nm)	Most dominant orbital transition	
431	HOMO-21	LUMO
	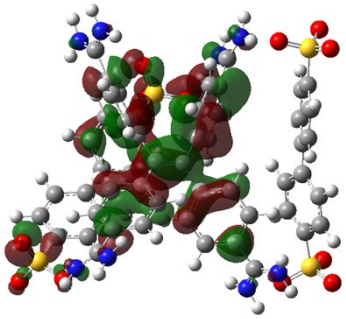	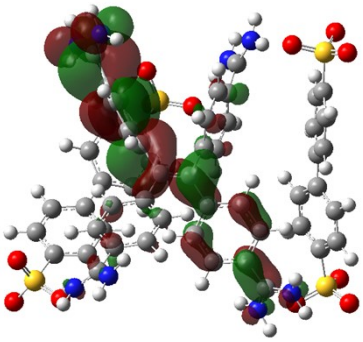
458	HOMO-11	LUMO
	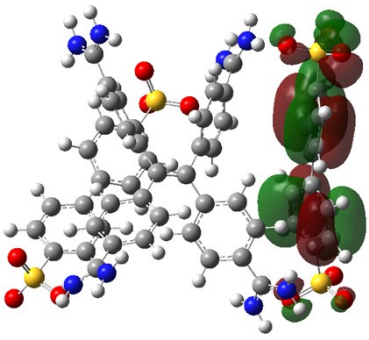	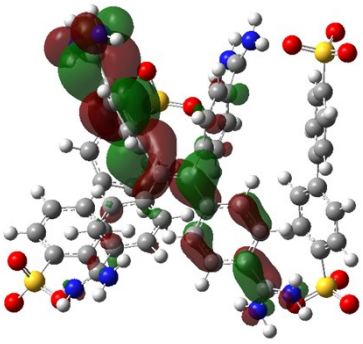

Table S4. Energy level of CPOS-9 and rare earth ions.

	Energy Level (eV)
CPOS-9	4.71 and 5.55
Ce^{3+}	6.17
Tm^{3+}	2.64
Pr^{3+}	7.58
Sm^{3+}	2.79
Dy^{3+}	1.62
Ho^{3+}	3.80
La^{3+}	17.77
Lu^{3+}	11.21
Nd^{3+}	2.66

Section 11. Crystallographic data

Table S5. Crystallographic data from the Single Crystal X-ray diffraction experiments.

	CPOS-9
Empirical formula	$C_{27}H_{24}N_4O_6S_2$
Formula weight	564.62
Temperature [K]	298.0
Crystal system	orthorhombic
Space group (number)	$Ccca$ (68)
a [Å]	17.8432(7)
b [Å]	52.7483(13)
c [Å]	12.5917(5)
α [°]	90
β [°]	90
γ [°]	90
Volume [Å^3]	11851.3(7)
Z	16
ρ_{calc} [gcm^{-3}]	1.266
μ [mm^{-1}]	2.011
F(000)	4704
Crystal size [mm^3]	0.1×0.1×0.1
Crystal colour	clear light colourless
Crystal shape	block
Radiation	CuK_α (λ=1.54184 Å)
2θ range [°]	3.35 to 137.39 (0.83 Å)
Reflections collected	52839
Independent reflections	5442 R_{int} = 0.1212 R_{sigma} = 0.0676
Completeness to θ = 67.684°	99.9 %
Data / Restraints / Parameters	5442/68/398
Goodness-of-fit on F^2	1.049
Final *R* indexes [$I \geq 2\sigma(I)$]	R_1 = 0.0608 wR_2 = 0.1750
Final *R* indexes [all data]	R_1 = 0.0766 wR_2 = 0.1911
Largest peak/hole [eÅ^{-3}]	0.51/−0.30

Crystal structure data can be obtained free of charge from the Cambridge Crystallographic Data Centre via https://www.ccdc.cam.ac.uk and have been allocated the accession numbers CCDC 2361305 (CPOS-9).

Section 12. Supporting Reference

S1. Crysalispro, *1.171.41.89*, Rigaku OD (2020).

S2. Sheldrick, G. M. SHELXT–integrated space-group and crystal-structure determination. *Acta Cryst.* **A71**, 3–8 (2015).

S3. Sheldrick, G. M. Crystal structure refinement with SHELXL. *Acta Cryst.* **C71**, 3–8 (2015).

S4. Dolomanov, O. V., Bourhis, L. J., Gildea, R. J., Howard, J. A. K. & Puschmann, H. OLEX2: A Complete structure solution, refinement and analysis program. *J. Appl. Cryst.* **42**, 339-341 (2009).

S5. Groom, C. R.; Bruno, I. J.; Lightfoot, M. P.; Ward, S. C. The Cambridge Structural Database. *Acta Cryst.* **B72**, 171–179 (2016).

S6. Jiang, H. et al. Fluorescent supramolecular organic frameworks constructed by amidinium-carboxylate salt bridges. *Chem. Eur. J.* **27**, 15006–15012 (2021).